Ann. Geophys., 26, 1905–1917, 2008
www.ann-geophys.net/26/1905/2008/

Annales Geophysicae

Using spectral characteristics to interpret auroral imaging in the 731.9 nm O^+ line

H. Dahlgren[1], N. Ivchenko[1], B. S. Lanchester[2], J. Sullivan[2], D. Whiter[2], G. Marklund[1], and A. Strømme[3,*]

[1]Space and Plasma Physics, School of Electrical Engineering, KTH, Stockholm, Sweden
[2]School of Physics and Astronomy, University of Southampton, UK
[3]SRI International, 333 Ravenswood Avenue, Menlo Park, CA-94025, USA
[*]previously at: EISCAT Scientific Association, P.O. Box 432, 9171 Longyearbyen, Norway

Received: 5 February 2008 – Revised: 30 May 2008 – Accepted: 5 June 2008 – Published: 15 July 2008

Abstract. Simultaneous observations were made of dynamic aurora during substorm activity on 26 January 2006 with three high spatial and temporal resolution instruments: the ASK (Auroral Structure and Kinetics) instrument, SIF (Spectrographic Imaging Facility) and ESR (EISCAT Svalbard Radar), all located on Svalbard (78° N, 16.2° E). One of the narrow field of view ASK cameras is designed to detect O^+ ion emission at 731.9 nm. From the spectrographic data we have been able to determine the amount of contaminating N_2 and OH emission detected in the same filter. This is of great importance to further studies using the ASK instrument, when the O^+ ion emission will be used to detect flows and afterglows in active aurora. The ratio of O^+ to N_2 emission is dependent on the energy spectra of electron precipitation, and was found to be related to changes in the morphology of the small-scale aurora. The ESR measured height profiles of electron densities, which allowed estimates to be made of the energy spectrum of the precipitation during the events studied with optical data from ASK and SIF. It was found that the higher energy precipitation corresponded to discrete and dynamic features, including curls, and low energy precipitation corresponded to auroral signatures that were dominated by rays. The evolution of these changes on time scales of seconds is of importance to theories of auroral acceleration mechanisms.

Keywords. Ionosphere (Auroral ionosphere; Particle precipitation; Instruments and techniques)

1 Introduction

Ground-based observations of active aurora have shown the prevalence of dynamic fine structure within auroral displays, often with sub-second time scales and sub-km filamentation. Recent instrumental development within this field has led to an increase in detailed studies concerning thin auroral arcs and filaments (Lanchester et al., 1997; Trondsen and Cogger, 1998; Semeter and Blixt, 2006). Imaging of the aurora provides information on auroral morphology, but little or no spectral information, which holds the key to the energy of the precipitation. Multispectral imaging is thus an important tool for understanding the processes that are responsible for the dynamics and spatial variations of auroral structures (Semeter et al., 2001).

Another type of instrument used for measuring auroral signatures is the imaging spectrograph, which may provide simultaneous measurements in the wavelength region of the imager filters. Pallamraju and Chakrabarti (2005) have used an imaging spectrograph named HIRISE to study daytime aurora at high spectral resolution, and Ivchenko et al. (2005) used the Spectrographic Imaging Facility (SIF) on Svalbard combined with incoherent scatter radar and optical measurements to investigate the $O^+\ ^4P - {}^4D^o$ multiplet in an electron aurora event. A spectrographic analysis of curls and rays (Ivchenko et al., 2004) showed that different emissions are present in different auroral configurations. The combination of multispectral measurements at high temporal resolution with spectrographic measurements for selected auroral events provides a very powerful tool for unravelling the changes in auroral signatures, both temporal and spatial. The result of combining such instruments, as well as the colocated ESR measurements is the subject of this paper.

During a substorm on 26 January 2006 over the EISCAT Svalbard Radar site (geographic coord: 78.1° N, 16.2° E, ILAT: 75.1°, MLT: UT+2:45) three different instruments measured the evolution of the auroral display simultaneously:

1. the Auroral Structure and Kinetics (ASK) instrument, a set of three narrow field of view low light imagers equipped with narrow interference filters, giving high

Correspondence to: H. Dahlgren
(hanna.dahlgren@ee.kth.se)

resolution information on the morphology of different emissions,

2. the Spectrographic Imaging Facility (SIF), consisting of a high resolution spectrograph to study four chosen wavelength regions simultaneously, and

3. the EISCAT Svalbard Radar (ESR) providing simultaneous electron density profiles of the ionosphere, as well as ion and electron temperature profiles.

One of the ASK filters selects the metastable $O^+(^2P)$ emission at 731.9 nm, which is produced by ionization of O atoms by electron precipitation of low energy (<1 keV). From this state, the $O^+(^2P–^2D)$ transitions give rise to the 731.9 nm and 733.0 nm emissions observed in aurora (Rees et al., 1982). These emissions have a life time of up to 5 s (Rees, 1989), making them a useful tool for measuring plasma flows in the ionosphere. However, the lines occur in the same spectral interval as the N_2 1 PG band, which, together with OH airglow, contaminates the measurements. It is therefore crucial to understand the spectral surroundings of the O^+ emission. The intensities of O^+, N_2 and OH emission detected with SIF have been analysed, and compared to the intensity of the O^+(731.9 nm) line as measured by ASK, to provide a measure of the contamination of other emissions than the O^+ emission in the ASK filter.

The 2-D images obtained with ASK provide detailed auroral morphology which is used in addition to the ESR electron density profiles to give a full description of the studied events. These profiles contain information about the energy distribution of the precipitating electrons. A clear indication of differences in morphology at times of different precipitation energies is found and discussed.

2 Instrumentation

2.1 ASK

The ASK instrument was designed to study the fine-scale aurora at a very high temporal and spatial resolution and relate the auroral morphology to the energy of the precipitation. The instrument consists of three narrow field high resolution cameras, each one equipped with an Electron Multiplying CCD (EMCCD) detector and a narrow band filter, centered on 562.0 nm (ASK1), 731.9 nm (ASK2) and 777.4 nm (ASK3). During the period studied here, only ASK2 and ASK3 were working. The field of view is $6.1°\times6.1°$, and the temporal resolution 5 frames per second (fps). ASK is located at the ESR site.

The ASK1 filter transmission curve is centered on 562.0 nm, with a Full Width Half Maximum (FWHM) of 2.6 nm, to let through emission from the O_2^+ 1N (2,0) bands. This provides a measure of high energy precipitating electrons.

The ASK2 filter lets through emission from the metastable oxygen ion doublet at 731.9 nm and 733.0 nm caused by the $O^+(^2P\text{-}^2D)$ transition. The filter transmission curve is centered on 732.0 nm and has a FWHM of 1.0 nm. This emission is a signature of low energy precipitation.

The ASK3 filter is centered on 777.4 nm with a FWHM of 1.5 nm. The emission at this wavelength originates from dissociation in the E-region (O_2+e^-) and from direct excitation in the F-region (O+e^-).

2.2 SIF

SIF consists of several instruments, including an Echelle spectrograph with a meridian slit of 8°, and an intensified CCD imager, referred to as TLC (The Little Camera). It has a field of view $12°\times16°$ and a cutoff filter at 645.0 nm (McWhirter et al., 2001). The time resolution is 2.8 fps. On this occasion the spectrograph was equipped with a mosaic filter with four panels (Chakrabarti et al., 2001; Dahlgren et al., 2008). Panel O^+(7319) allows spectra in the region of 728.0–740.0 nm to be recorded. Two other SIF panels are of interest for this study. Panel O_2^+(5620) covers the wavelength interval 558.0–565.0 nm and detects the (1,0) transition of the O_2^+ first negative bands. Panel O(8446), isolates an oxygen line that is produced by the same mechanisms as the 777.4 nm emission detected in ASK3. The integration time of the spectrograph in this study is 30 s.

Absolute intensity calibration of ASK was achieved by comparing measured intensities of solitary stars in the cameras with their tabulated fluxes. A similar method using star intensities was used for the SIF absolute intensity calibration. SIF is placed at the Auroral Station in Adventdalen, located 7 km north-west of the ESR site.

2.3 ESR

Height profiles of the electron density in the ionosphere are obtained with the EISCAT Svalbard Radar. The present observations were made with the 42-m UHF antenna, which is pointed along the local magnetic field line. The radar beam has a half power beam width of 1.8 degrees (Markkanen et al., 2006). The radar programme “Steffe” was used, which is a multipurpose E and F layer experiment with fully decoded gates from 105 to 216 km and from 259 to 965 km. The range resolution is 1 km and the time resolution 6.4 s.

2.4 All-sky camera

For the event presented in this study, data from the University of Alaska all-sky imager was also used, to provide information on the larger-scale auroral morphology. It is an intensified CCD television camera, recording at a rate of 30 frames per second. The camera was operating from the Auroral Station in Adventdalen.

3 Method for separating SIF spectral components

One of the primary goals of this investigation was to characterise the spectral intensity of the O^+ emission and its spectral surroundings, and thus determine the amount of contamination from other species in ASK2. This is done by analyzing the spectral region provided by SIF panel O^+(7319). As well as the main species of interest, this panel measures emission from the N_2 1PG (6,4) and (5,3) bands and the (8,3) Meinel band of OH airglow. The N_2 1PG (6,4) band has its head at 727.4 nm and the (5,3) band at 738.7 nm. The N_2 1PG emission peaks at about 110 km altitude, whereas the O^+ emission is from above 200 km. When observing in a direction across the field line, the geometry can be used to separate the emissions. Semeter (2003) used the difference in emission heights to separate the O^+ emission from the N_2 1PG band. Sullivan et al. (2008) have also used this method to distinguish between low and high energy precipitation and the related optical signatures in the ESR beam, using a camera located with SIF, 7 km away from the radar. For spectra and rotational temperatures of the N_2 1PG band, see Sivjee et al. (1999). Airglow from the hydroxyl band, OH (8,3) (spectrum shown in Fig. 7.2.5. in Rees, 1989), also contributes to the contamination of O^+ measurements. The OH (8,3) band emission profile peaks at an altitude of just above 90 km (McDade et al., 1987). Throughout this study it has been assumed that the rotational as well as vibrational temperature of the N_2 1PG and OH (8,3) bands are constant and thus do not affect the overall shape of these spectra in the wavelength interval of interest.

Since the spectra for the above emissions have different shapes, the measured spectra can be modelled as a weighted sum of reference spectra corresponding to each emitting species. Rather than using synthetic spectra, reference spectra have been found in the SIF dataset at times when each emission dominates. This is determined by comparing the integrated intensity in the wavelength interval 738.0–738.5 nm, which is the region of the strongest N_2 emission in the observed spectra, with the integrated intensity in the wavelength interval 731.9–732.1 nm, which is the interval of the strongest O^+ emission line. The reference spectra for all species were taken from 26 January 2006. Figure 1 shows the three reference spectra and a sample total spectrum built up from the weighted sum of the reference spectra for O^+, N_2 and OH emissions. The reference spectrum for N_2 1PG was taken at 18:06:56 UT, with 30 s exposure time. At this time the ratio of the measured O^+ and N_2 intensities is 0.35, the lowest value measured in this data set at the same time as the nitrogen emission exceeded the threshold value chosen to ensure an adequate signal to noise ratio for N_2. The spectrum is shown in Fig. 1a. The reference spectrum for O^+ (7319) emission was taken at 17:28:02 UT, also with 30 s exposure. A background level has been removed from this reference spectrum, as well as some weak contamination from the N_2 1PG band that was present at this time. The corresponding spectrum is shown in Fig. 1b. The intensity ratio between the 731.9 nm and 733.0 nm O^+ lines has been investigated in terrestrial as well as astrophysical environments (e.g. Sharpee et al., 2004; De Robertis et al., 1985). From this reference spectrum, the ratio of these two O^+ emission lines is found to be 1.6. Figure 1c shows the reference spectrum for the background and the OH band, which was obtained from a later time interval when the auroral activity had reduced to a minimum. The spectra were integrated between 19:22:14 UT and 20:12:48 UT. In this spectral interval emission lines at 730.4 nm, 731.6 nm, 733.0 nm, 734.1 nm, 735.9 nm and 736.9 nm of the (8,3) Meinel band of OH airglow can be identified. Each data spectrum from the SIF O^+ (7319) panel was then fitted by weighted combinations of the N_2, cleaned O^+ and OH and background reference spectra. Figure 1d is an example of a weighted reference spectra and the measured spectrum (black) for the time 17:35:06 UT. At this time, N_2 is weighted by a factor 0.23 (blue), O^+ a factor 0.76 (green) and OH a factor 0.0090 (orange) to fit to the total spectrum. The ASK2 filter transmission curve is also plotted (in purple) in the figure.

This analysis provides a method for estimating the contribution made by each emission in the ASK2 images, by comparing them with the intensities of different emissions recorded by the spectrograph. The main drawback is the much lower temporal resolution (30 s integration for these data) of SIF, which limits the ability to analyse rapid morphological variations. Despite this, the spectrographic data provide important information on how to interpret the emissions detected in ASK2.

4 Application to events from 26 January 2006

During one substorm on 26 January 2006, ASK, SIF and ESR measured the evolution of ionospheric activity, which started at 17:00 UT and continued until 19:00 UT. An overview of the interval is shown in Fig. 2, where the first panel is electron density height profiles between 90–250 km obtained with the ESR. Intervals of increased electron density in the E region ionosphere can be identified. Above this panel, snapshots from the Alaska All-Sky imager show the large scale auroral evolution of the substorm. North is up in these images. The second and third panels show keograms from ASK2 and ASK3 cameras, created by forming a time series of slices of central pixels from ASK images at 2 s integration. Panels 4 and 5 contain spectrographic data from SIF for the same time interval. Panel 4 is the time history of SIF spectra for O^+(7319), and panel 5 is SIF spectra for O_2^+(5620). The optical emissions are accompanied by simultaneous enhancements in the ionospheric density as seen in the radar panel.

The all-sky data from this period show aurora appearing in the south at about 17:20 UT, then slowly moving to the north. At 17:30 UT the aurora has reached magnetic zenith,

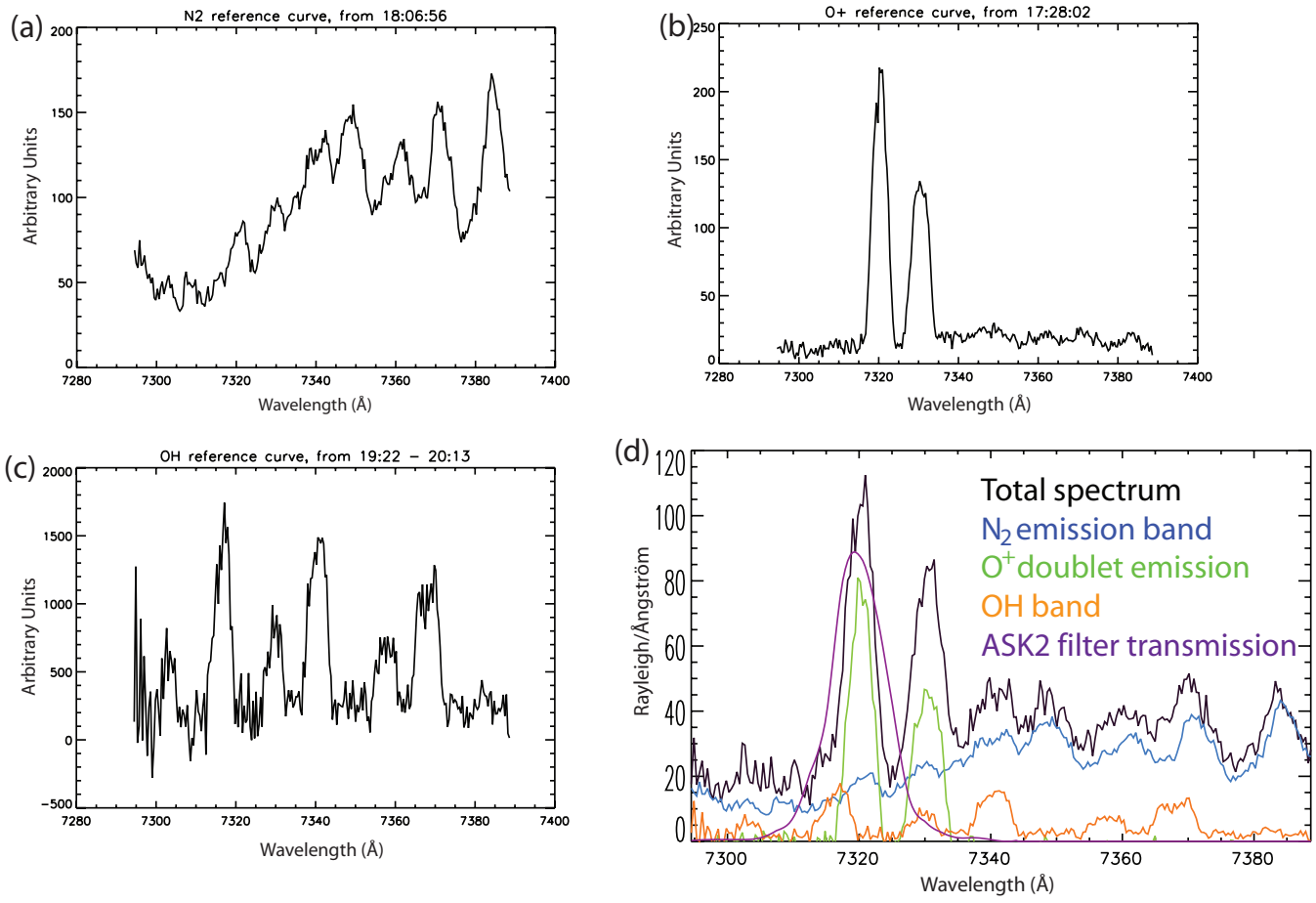

Fig. 1. Reference spectra for **(a)** N_2 1PG band, **(b)** O^+ and **(c)** OH band, obtained from SIF data, at times when only one emission dominates the total spectra. By weighting the reference spectra it is possible to determine how much each emission contributes to the resultant spectrum. **(d)** shows the weighted reference spectra and the resultant spectrum (black) for the time 17:35:06 UT.

where coronal rays are formed. This is the expansion phase of the substorm, and the coronal aurora becomes highly intense during event 1 marked in Fig. 2. The activity decreases, but an auroral arc with folds forms to the west, and moves through the ASK and ESR field of view at 17:42 UT (event 2). During event 3 the auroral emission is returning from north to south again, and an intense arc with curls is drifting past magnetic zenith, followed by coronal rays. At event 4, around 17:50 UT, the aurora is expanding to the north again, filling a large part of the sky with bright emission and dynamic structures.

The aim of this investigation is to compare the brightness of 731.9 nm O^+ line emission detected in ASK2 with the composition of the spectral data in the region of this wavelength measured by SIF. The ASK2 emission brightness is obtained by averaging the brightness in all pixels inside a circular region in the ASK field of view, centered on magnetic zenith (180.7° east of north, 81.7° elevation) with a radius of 0.9 degrees, corresponding to the half power beam width of the ESR radar (Markkanen et al., 2006). The first panel in Fig. 3 shows these ASK2 (O^+) emissions in black. The green line is the sum of O^+ and N_2 emissions detected in the SIF panel O^+(7319), integrated with the ASK2 filter transmission curve, for the two hour time interval. From this plot it can be concluded that emissions detected in ASK2 and SIF panel O^+(7319) show a good agreement, although there are some deviations, most likely due to the slight difference in the fields of view of the SIF slit and the area of the radar beam mapped on the ASK images. The ASK2 data is in general brighter than the sum of O^+ and N_2 emissions, since it contains a background which has been removed from the SIF data.

The second panel of Fig. 3 demonstrates the separation of the components of SIF panel O^+(7319) and shows which emission dominates at each time. Normalised intensities of $O^+$and N_2 from SIF are shown in green and blue respectively. The intensity of O detected in ASK3 is plotted in the same panel in black, and the intensity of O_2^+ 1N from SIF

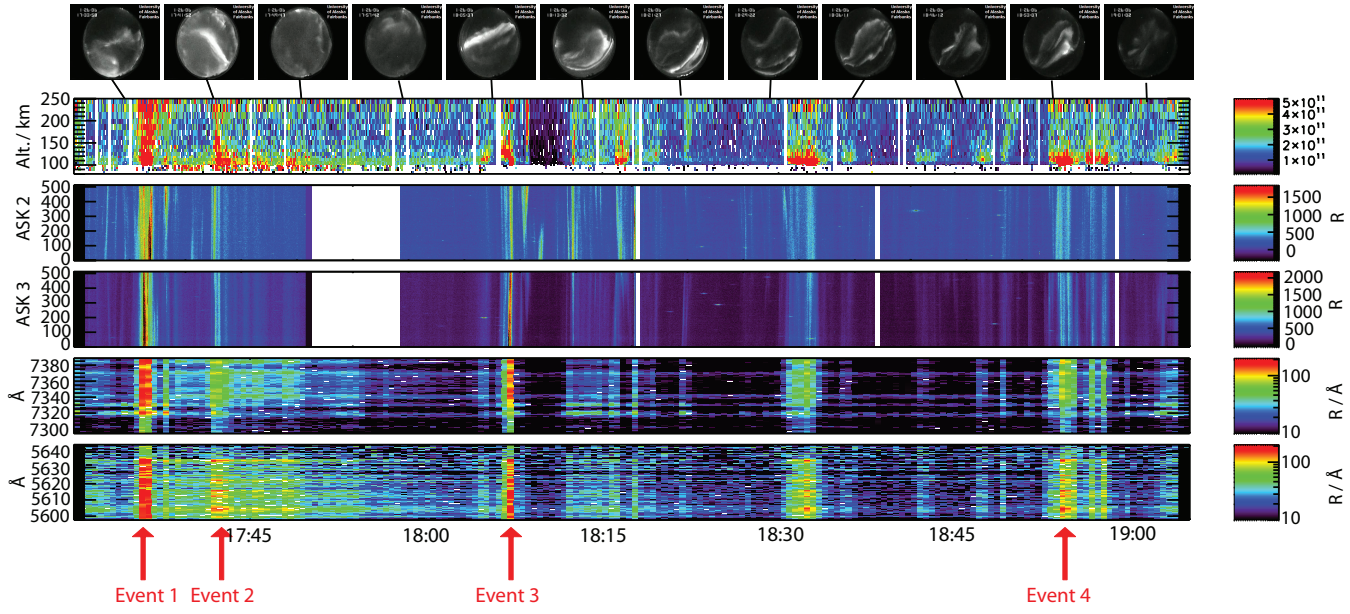

Fig. 2. Overview of the interval 17:30 UT to 19:00 UT on 26 January 2006. Top: Images from the University of Alaska All-Sky imager, panel 1: ESR electron density vs altitude, panel 2 and panel 3: ASK2 and ASK3 keograms, panel 4: spectrographic data from SIF O^+(7319), panel 5: spectrographic data from SIF O_2^+(5620). The events discussed in Sect. 4 are marked with red arrows.

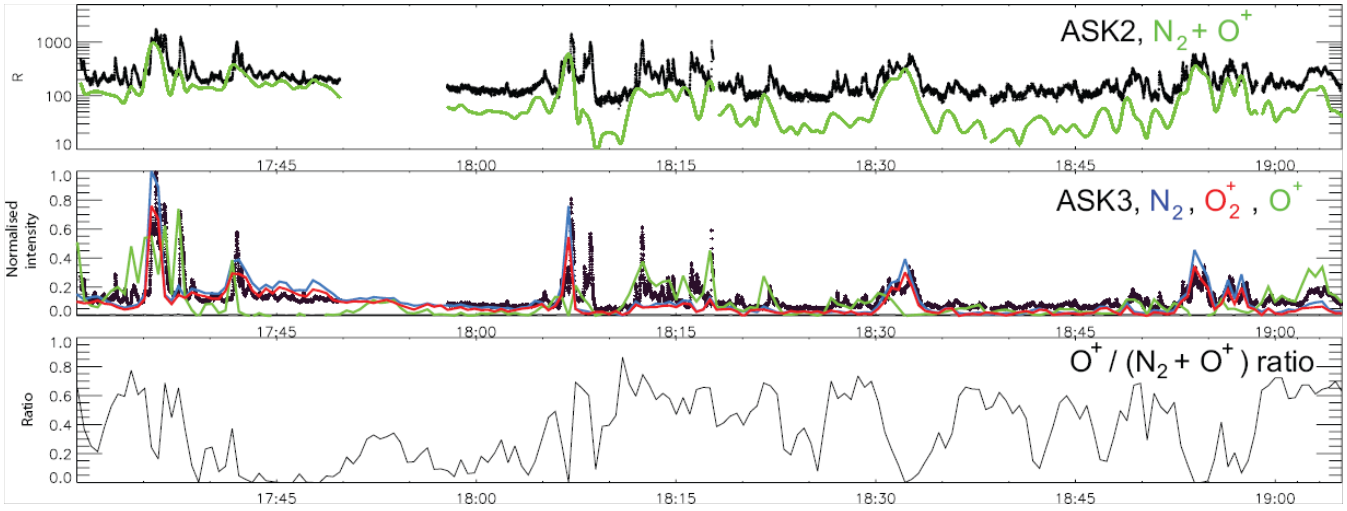

Fig. 3. Comparison of emissions in ASK and SIF for the interval 17:30 UT to 19:00 UT on 26 January 2006. Panel 1: Emission detected in the centre of ASK2 (black) and the sum of O^+ and N_2 emissions in SIF O^+(7319) (green). Panel 2: Normalized intensities of O^+ (green) and N_2 (blue) from SIF spectra from O^+(7319), intensity of O detected in ASK3 (black) and O_2^+ emission in SIF spectra from O_2^+(5620) (red). Panel 3: Ratio of $O^+/(N_2 + O^+)$ illustrates when emissions in ASK2 were caused mainly by O^+ emission rather than the contaminant N_2 1PG band.

(see Fig. 2) is in red. These two emissions provide information about the energy carried by the precipitating electrons, since O_2^+ 1N emission is caused by high energy precipitation whereas O can be produced by both high and low energy. The emissions thus contribute to understanding the optical signals in ASK2 spectrally.

Using this method of separating emission intensities, it is possible to estimate the amount of emission in ASK2 that is caused by O^+ as distinct from that which is caused by contamination from N_2. This is demonstrated in the third panel of Fig. 3 where the ratio of O^+ emission to the sum of O^+ and N_2 emissions has been plotted. Note that for most periods of

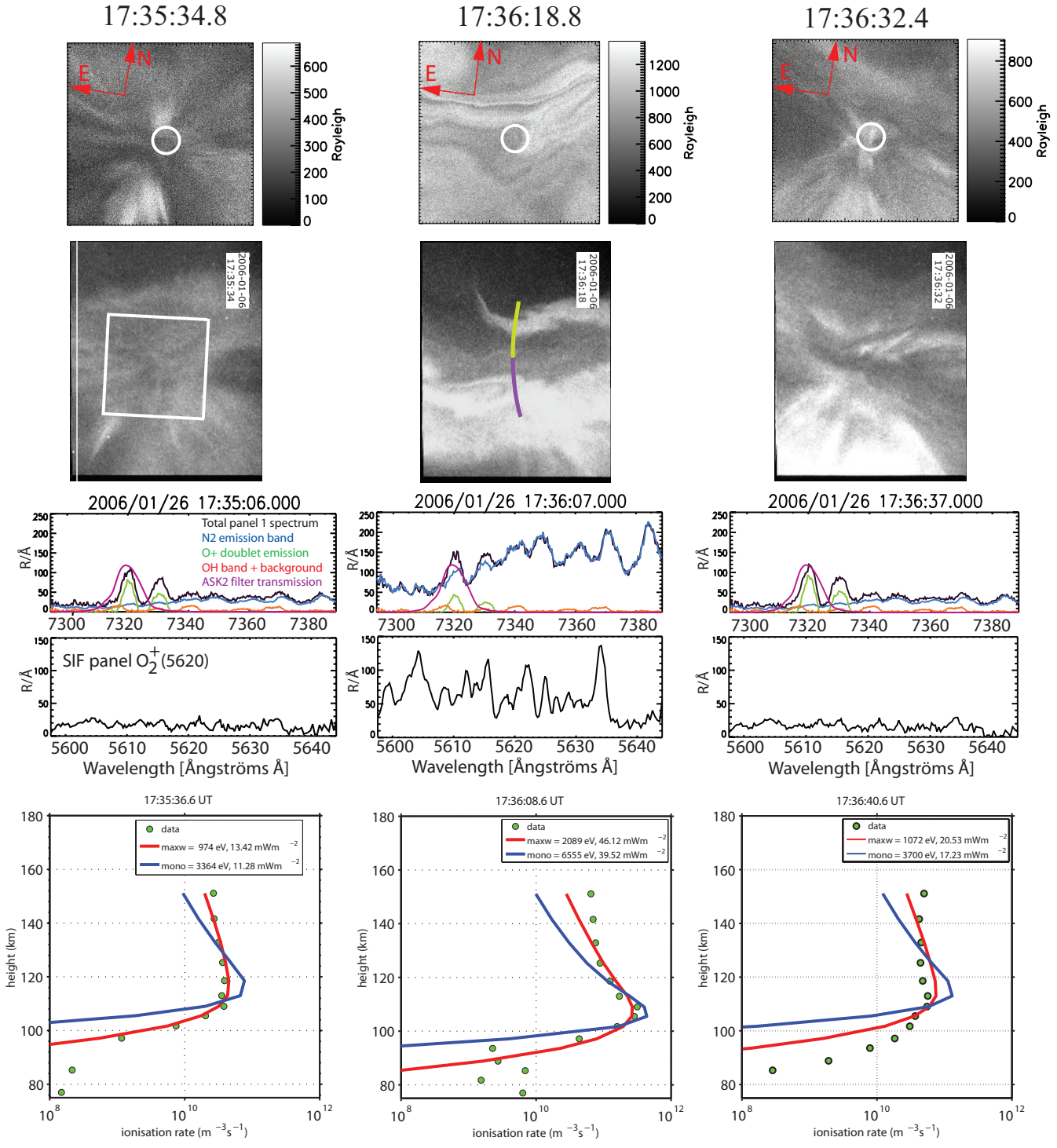

Fig. 4. Event 1: Optical and electron density data for three times from 17:35:00. The top row shows ASK3 images, the second row SIF video camera images, the third and fourth rows the SIF spectra. The bottom row are ionisation rate profiles derived from the ESR electron density profiles, and best fit model profiles with assumed Maxwellian and monoenergetic energy distributions. The ESR radar beam is indicated with circles in the ASK images. The ASK field of view is marked in the first SIF video camera image, and the HiTIES slit is marked in the second image.

intensified signals in ASK2 and ASK3 (black lines in panels 1 and 2 respectively) there is a dip in the $O^+/(O^+ + N_2)$ ratio, indicating that high energy contamination is present in ASK2. The details of these changes will be considered during events labelled 1–4 in Figs. 2 and 3. These four short time intervals of auroral brightenings have been selected to study the morphology of small scale filaments and how they relate to their spectral signatures, and in particular the O^+ emission.

Event 1: The top row of panels of Fig. 4 shows three ASK3 images within one minute from 17:35:34 UT. Marked as a circle in the images is the size and position of the radar beam, and the north and east directions are indicated with arrows. To put the narrow field of view ASK images into a larger perspective, images from the SIF video camera from the same times are displayed in the second row of panels. The TLC video camera has a field of view of 12° (east-west) ×16° (north-south), compared to the ASK field of view of 6.1°×6.1°, which is marked with a white square in the first TLC image. In the central TLC image the position of the SIF spectrograph slit is indicated, with panels $O^+(7319)$ and $O_2^+(5620)$ coloured purple and panel O(8446) coloured yellow. At the beginning and end of this interval, rays stretching out in different directions from the magnetic zenith are seen in the ASK images. However, 40 s later, at about 17:36:18 UT, the aurora changes into coherent, narrow, filamentary structures, that are highly dynamic. After another 12 s (at 17:36:32 UT) rays reappear in the field of view. The next two rows of panels show SIF spectra from $O^+(7319)$ and $O_2^+(5620)$ for time intervals close to or overlapping the times when the ASK and video camera images were obtained. The black lines correspond to the total SIF spectrum in each panel. By using the separation method of Sect. 3, the emission curves for the different species can be obtained. During the first and third selected times the O^+ doublet (green) dominates the spectra, whereas this emission is overwhelmed by emission from the N_2 band (blue) at the central time. The intensity of the SIF O_2^+ emission is stronger at the central time, when the N_2 band was also dominating the $O^+(7319)$. At this time, the total intensity in the region of the O_2^+ lines reaches values of almost 150 R/Å.

The above changes in the optical signatures can be compared with EISCAT electron density height profiles, which have been used to estimate the changes in peak energy and energy flux. Figure 5 shows a time series of the radar profiles in the bottom panel for event 1 at 6.4 s resolution. A profile inversion function (Palmer, 1995) based on the flux-first fitting algorithm described in Lanchester et al. (1998) has been used. An ionisation rate profile inferred from the radar data for an assumed recombination rate coefficient is matched against model ionisation rate profiles for the E region. For the modelled rate profiles two "libraries" are used. These have been calculated for electron spectra with Maxwellian, and monoenergetic (approximated by 10 percent half-width Gaussian) spectral shapes of varying peak energy, respectively. In both cases a downward flux of 1 mW m^{-2} is used. The libraries are generated using an auroral ion-chemistry model (Lanchester et al., 2001). All the spectra are isotropic, and a neutral atmosphere obtained from MSIS90 (Hedin, 1991) is used. Examples of the best fits corresponding to the three times selected in event 1 are shown in the bottom row of panels in Fig. 4. It can be seen that during the first and last time intervals, measured profiles are flat, and do not have a peak in the E region. They are fitted better by Maxwellian than monoenergetic spectra, and have lower fluxes. These profiles correspond to times when long rays were seen in the images. The central interval has a clear peak superimposed on the profile at 105–110 km, which is fitted better by a monoenergetic spectrum of peak energy 3.7 keV. This corresponds to the time of narrow arc filaments in the images of Fig. 4.

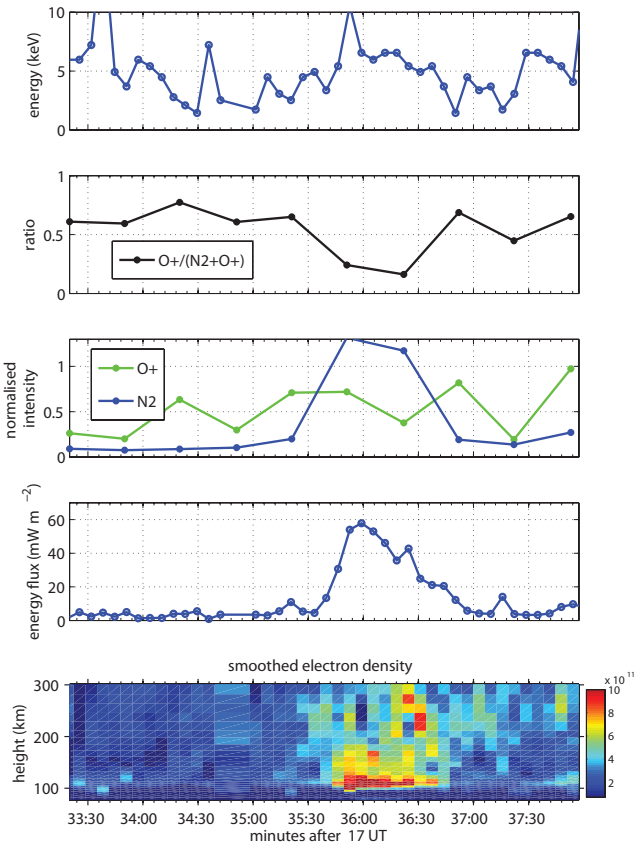

Fig. 5. Electron transport model results compared with optical results: Panel 1: peak electron energy for event 1, when assuming the input electron spectrum at the top of the ionosphere to be monoenergetic, Panel 2: $O^+/(O^+ + N_2)$ ratio, Panel 3: O^+ intensity (green) and N_2 intensity (blue), Panel 4: fitted energy flux below 150 km, Panel 5: Smoothed electron density height profiles.

The fitting process was carried out for the whole interval. The top panel of Fig. 5 gives the changes in the peak

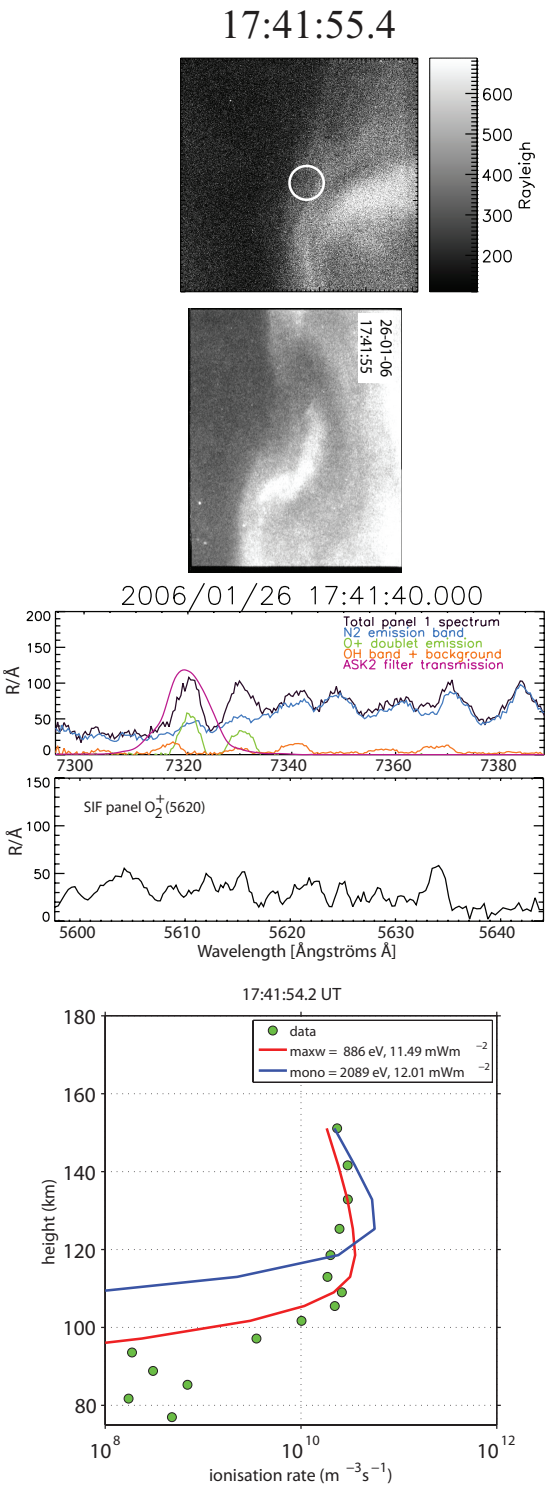

Fig. 6. Event 2: Optical and electron density data from 17:41:55 UT. The top image is ASK3, the second is a SIF video camera image, the third and fourth rows the SIF spectra. The bottom row are ionisation rate profiles derived from the ESR electron density profiles, and best fit model profiles with assumed Maxwellian and monoenergetic energy distributions.

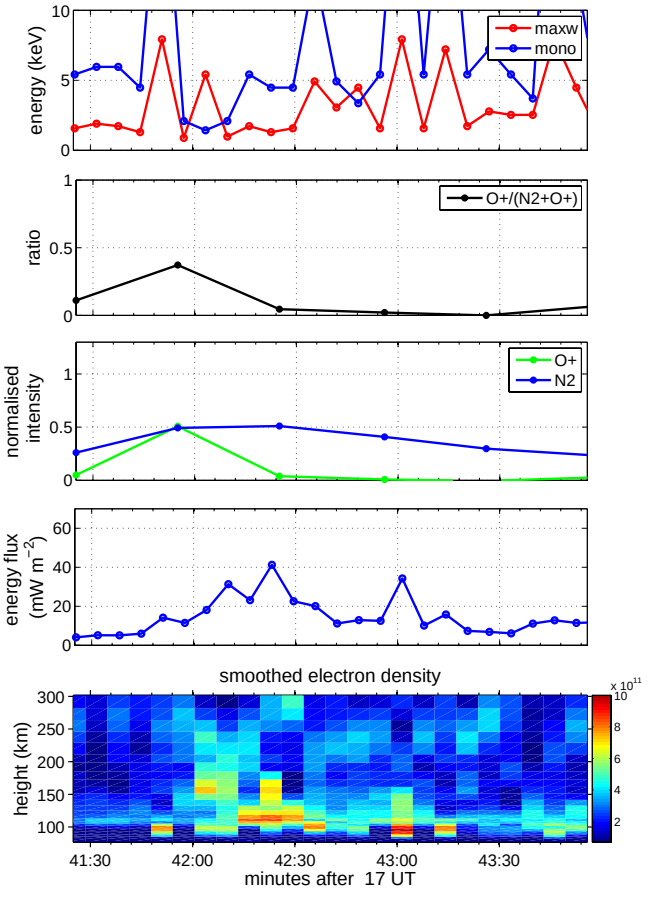

Fig. 7. Electron transport model results compared with optical results: Panel 1: peak electron energy for event 2, when assuming the input electron spectrum at the top of the ionosphere to be monoenergetic, Panel 2: $O^+/(O^+ + N_2)$ ratio, Panel 3: O^+ intensity (green) and N_2 intensity (blue), Panel 4: fitted energy flux below 150 km, Panel 5: Smoothed electron density height profiles.

energy for a monoenergetic spectrum fitted to the radar profiles, thus highlighting the times with energetic precipitation. The fourth panel gives the resultant flux from the E region. For a monoenergetic spectrum, the energies are around 5 keV during the time of the arc filaments, with one interval with a peak energy of more than 10 keV. The optical signatures during these changes are shown in panel 3, which is the separated SIF emission for O^+ and N_2. The O^+ intensity is strong throughout, but the N_2 increases dramatically for less than one minute. The changes in the $O^+/(O^+ + N_2)$ ratio are plotted in the second panel. It can be seen that this event begins with low energy precipitating electrons, then changing into high energy precipitation for a short while, before going back to low energy precipitating electrons, as found by Dahlgren et al. (2008).

Event 2: A few minutes later at 17:41:55 UT there is another increase in electron density measured over the height

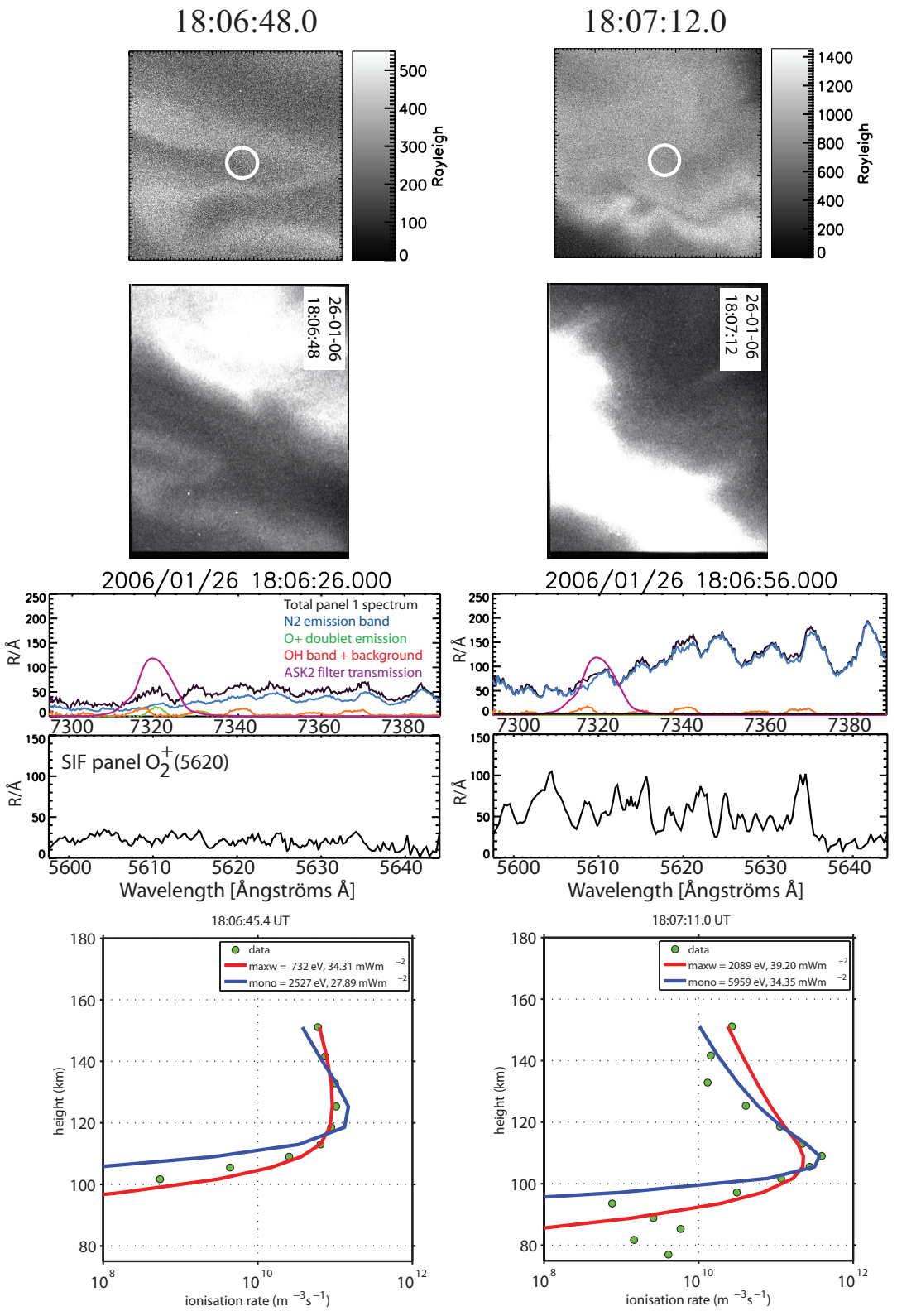

Fig. 8. Event 3: Optical and electron density data from 18:06 UT. The top row shows ASK3 images, the second row SIF video camera images, the third and fourth rows the SIF spectra. The bottom row are ionisation rate profiles derived from the ESR electron density profiles, and best fit model profiles with assumed Maxwellian and monoenergetic energy distributions.

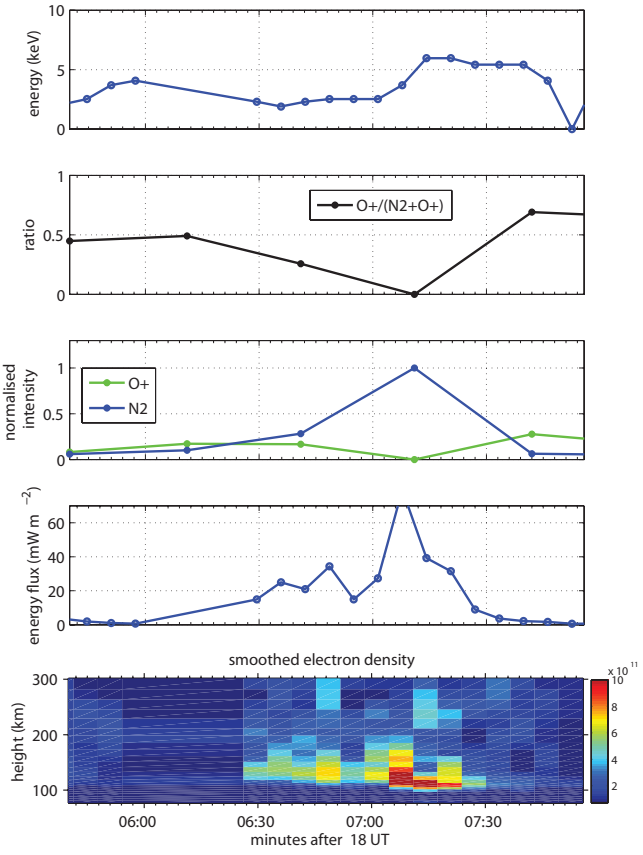

Fig. 9. Electron transport model results compared with optical results: Panel 1: peak electron energy for event 3, when assuming the input electron spectrum at the top of the ionosphere to be monoenergetic, Panel 2: $O^+/(O^+ + N_2)$ ratio, Panel 3: O^+ intensity (green) and N_2 intensity (blue), Panel 4: fitted energy flux below 150 km, Panel 5: Smoothed electron density height profiles.

range 100–200 km. Figure 6 shows images from ASK and the SIF video camera which both recorded auroral rays at the beginning of the event. A large-scale arc with folds then passed the field of view of ASK and the detected emissions in the imagers became more structured. The spectral data shown in the third and fourth panels show that this event is rich in both N_2 and O^+ emission. Figure 7, similarly to Fig. 5, compares the changes in the radar profiles and the optical signatures during this event. The results of the above fitting process are less clear in this event, as the radar profiles have a combination of intense peaks in the low E region, and increases in density at heights around 150 km. The fitting process is applied only to the lower E region. One profile at the start of the event is shown in the bottom panel of Fig. 6. The flat profile is clearly made up of more than one distinct shape, but is not fitted well by either curve. Both Maxwellian and monoenergetic energies have been included in the first panel of Fig. 7, since they do not vary in the same way throughout the event. The optical emissions in the third panel show the clear change in mixed O^+ and N_2 emission intensity at the start of the event (rays) to more dynamic and arc-like structures rich in N_2. The $O^+/(O^+ + N_2)$ ratio rises to 0.37 when rays are in the images, and decreases to zero as the arc filaments dominate.

Event 3: Twenty five minutes later another increase in auroral precipitation took place, at 18:06 UT. Images from ASK and SIF are shown in Fig. 8, as well as the SIF emissions in the same format as for the previous events. ASK3 (top) shows one narrow fold in the field of view at the beginning of this event. Seconds later an arc with curls along its length drifted through the magnetic zenith. Unfortunately the SIF video camera images taken at this time are saturated, but the structures detected by ASK3 can still be identified. The emissions during this event are mainly from N_2 and O_2^+, and only a very small fraction originate from O^+. The radar measurements shown in the bottom panel of Fig. 9 confirm that this event is the result of high energy precipitation, with the peak of the electron density decreasing from 120 km to 110 km during less than one minute. This decrease can be seen as an increase in the peak energy of the precipitation (top panel). The optical data from SIF indicates a large increase in N_2 during this interval, and a consequent reduction of the $O^+/(O^+ + N_2)$ ratio to zero from values of 0.5. There is some evidence again of a small increase in O^+ emission before and after the high energy event. The changes in the electron density profiles and fitted spectra are shown in the bottom row of panels in Fig. 8. The first profile is fitted better by a Maxwellian input spectrum, but a clear change occurs as the energy increases and the precipitation reaches to lower heights, making a better fit to a monoenergetic input spectrum.

Event 4: Intensifications can be seen in the ASK keograms and SIF spectra within a two minute interval starting at 18:53 UT and shown in Fig. 10. ASK3 images (top) contain auroral arcs and filaments. The same structures are found in the SIF images below. The spectral data from SIF show a strong signal from N_2, whereas the oxygen doublet is at the noise level. N_2 is the dominant emission during this event. Again the radar data shown in Fig. 11 give clear evidence that high energy precipitating electrons are dominant, with a well defined peak in the electron densities at about 105–110 km, and fitted peak energies of greater than 5 keV. Note that the energy flux is smaller during this event, indicating that there are fewer low energy electrons than in previous events. This is borne out by the optical data, which show that there is virtually no O^+ emission, and therefore a $O^+/(O^+ + N_2)$ ratio of zero for most of the event. Two sample profiles with fitted curves are shown in the bottom row of panels in Fig. 10.

5 Discussion

The strength of the ASK instrument is its high spatial resolution and high frame rate, which provides detailed information

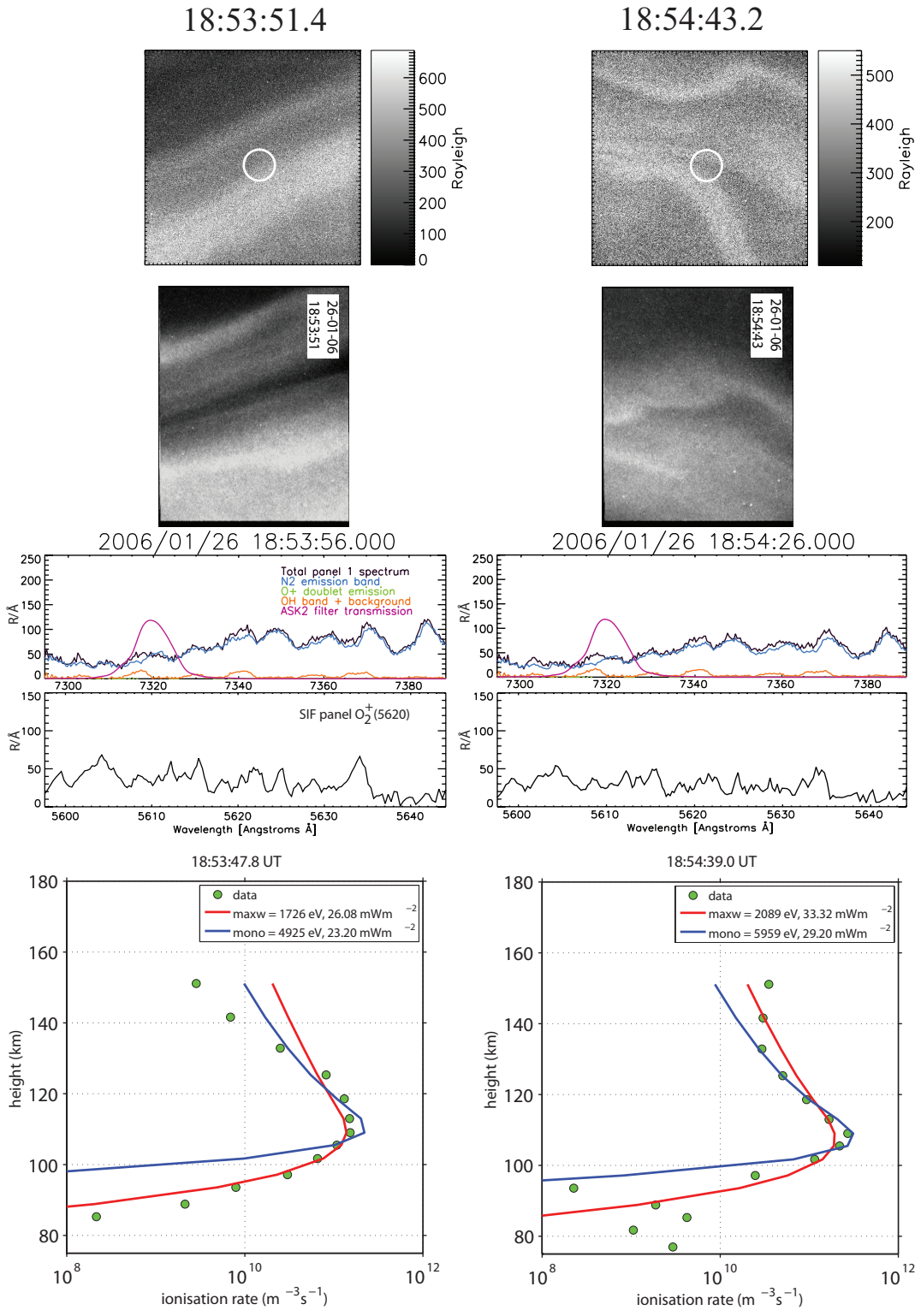

Fig. 10. Event 4: Optical and electron density data from 18:53 UT. The top row shows ASK3 images, the second row SIF video camera images, the third row ESR electron density profiles, and the fourth row SIF spectra. In the video camera images the position of the spectrographic slit is plotted, and the part with the mosaic filter letting through emissions at 732.0 nm is marked in red.

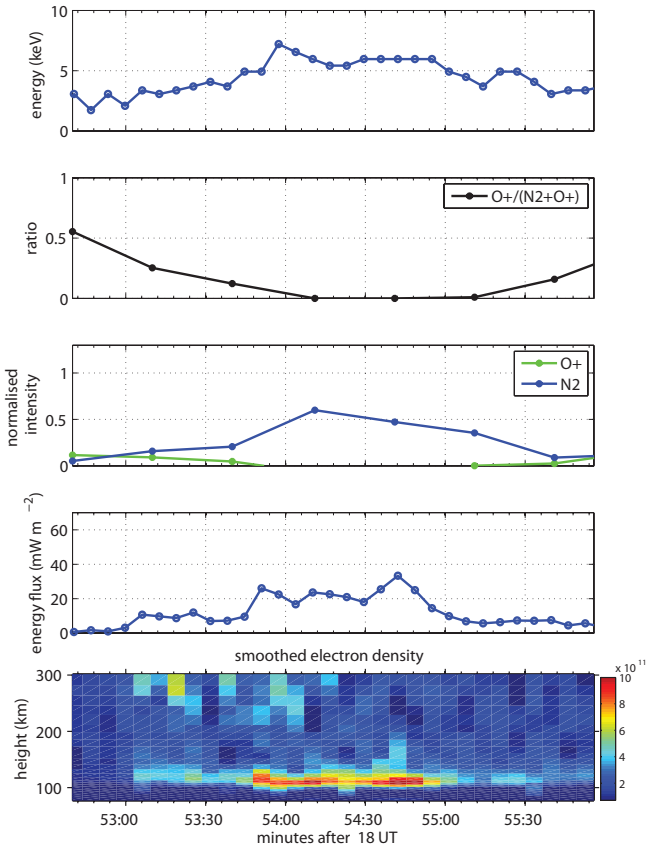

Fig. 11. Electron transport model results compared with optical results: Panel 1: peak electron energy for event 4, when assuming the input electron spectrum at the top of the ionosphere to be monoenergetic, Panel 2: $O^+/(O^+ + N_2)$ ratio, Panel 3: O^+ intensity (green) and N_2 intensity (blue), Panel 4: fitted energy flux below 150 km, Panel 5: Smoothed electron density height profiles.

on the 2-D auroral morphology. Since ASK is simultaneously imaging the aurora in three selected emission lines, it is capable of inferring small-scale variability in auroral electron precipitation, as demonstrated in Dahlgren et al. (2008). During two hours of substorm activity on 26 January 2006, four events have been examined in detail. Extended and well developed arcs or arc filaments are found during high energy precipitation, whereas periods with mixed high and low energy precipitation are characterised by aurora that is less coherent. At these times, the 2-D images contain discrete and separated features, such as the bundle of rays at 17:36:32.4 UT in Fig. 4. Such features are not typical for arc-like extended filaments present during high energy aurora. This is in agreement with Ivchenko et al. (2005).

With the ability to separate emissions in the SIF spectra, it is possible to study the relation between nitrogen emission and emission from the oxygen doublet in the ASK2 filter, and compare these results with the morphology of the aurora. In the events studied here, the nitrogen emission is found to dominate over the oxygen emission at times when there is a clear peak in electron density in the E-region, and the aurora exhibits intense, dynamic, clearly developed arc structures. However, when low energy precipitation is present in the aurora, the 731.9 nm filter used in ASK2 is efficient at imaging the forbidden O^+ emission.

Two types of precipitation have been considered: high energy electrons of several keV and low energy electrons responsible for producing emissions of O^+, which have energies in the range 100–200 eV. However, this simplified picture is not realistic. In event 1 there is a mixture of high and low energies at the central time. In event 2 the mixture is even more pronounced at the start of the event as the auroral structures move into the field of view. In event 3, for example at 18:06:48 UT (see Fig. 8), the energy of precipitation increases gradually over an interval of 25 s, with a corresponding change in the optical signatures. The spectral data from SIF contain more contributions from different emissions at the start of this time, and the SIF panel $O_2^+(5620)$ is noisier. As the precipitation hardens, the SIF spectrum becomes dominated by N_2 1PG emission and a fold in the arc within the field of view develops an instability in terms of curls along its length. In these three events it is clear that the precipitation patterns are complex in energy, in both space and time. Event 4, however, is a clear case of high energy precipitation, with little contribution from low energies. The unravelling of such information is necessary as input to theoretical models of auroral acceleration processes, in which the energy variations must be incorporated.

6 Conclusion

ASK and SIF have been calibrated independently, and a comparison between the intensities measured in the different instruments is illustrated in the two first panels of Fig. 3. It is found that emissions in ASK2 and the sum of N_2 and O^+ emissions in SIF panel $O^+(7319)$ follow each other closely (Fig. 3, top panel).

The ASK2 system is designed to study the auroral emission caused by the forbidden oxygen ion at 731.9 nm. However, although the transmission curve of the filter has a FWHM of only 1.0 nm, other emissions in this spectral range also contribute to the signal in ASK2, such as the N_2 1PG band and OH airglow. We describe a method to determine this amount of contamination by analysing simultaneous spectra from SIF. We find that an enhancement in N_2 emission occurs at the times when the detected aurora in ASK contains intense and well developed arcs or arc filaments. One of the aims of the ASK instrument is to study flows and afterglows of the forbidden oxygen doublet detected in the ASK2 filter. For this study it is crucial to be able to separate the contamination from the signal in this ASK filter.

Acknowledgements. Work at the Royal Institute of Technology was partially supported by the Swedish National Space Board and the Alfvén Laboratory Centre for Space and Fusion Plasma Physics. N. Ivchenko is supported by the Swedish Research Council. J. Sullivan was supported by, and the ASK instrument was funded by the PPARC of the UK. The University of Alaska all-sky camera data were provided by Charles Deehr of the Geophysical Institute, supported by NSF Grant ATM 0334800. The instrument was operated and maintained by Jeff Holmes of the University Centre in Svalbard. We also wish to thank the EISCAT and SIF/ASK campaign teams.

Topical Editor M. Pinnock thanks two anonymous referees for their help in evaluating this paper.

References

Chakrabarti, S., Pallamraju, D., Baumgardner, J., and Vaillancourt, J.: HiTIES: A High Throughput Imaging Echelle Spectrograph for ground-based visible airglow and auroral studies, J. Geophys. Res., 106, 30 337–30 348, 2001.

Dahlgren, H., Ivchenko, N., Sullivan, J., Lanchester, B. S., Marklund, G., and Whiter, D.: Morphology and dynamics of aurora at fine scale: First results from the ASK instrument, Ann. Geophys., 26, 1041–1048, 2008, http://www.ann-geophys.net/26/1041/2008/.

De Robertis, M. M., Osterbrock, D. E., and McKee, C. F.: The splitting of the 2s(2)2p(3) 2P term in O II, Astrophys. J., 293, 459–462, doi:10.1086/163251, 1985.

Ivchenko, N., Rees, M. H., Lanchester, B. S., Lummerzheim, D., Galand, M., Throp, K., and Furniss, I.: Observation of O+ (4P–4D0) lines in electron aurora over Svalbard, Ann. Geophys., 22, 2805–2817, 2004, http://www.ann-geophys.net/22/2805/2004/.

Ivchenko, N., Blixt, E. M., and Lanchester, B. S.: Multispectral observations of auroral rays and curls, Geophys. Res. Lett., 32, L18106, doi:10.1029/2005GL022650, 2005.

Lanchester, B. S., Rees, M. H., Lummerzheim, D., Otto, A., Frey, H. U., and Kaila, K. U.: Large fluxes of auroral electrons in filaments of 100 m width, J. Geophys. Res., 102, 9741–9748, 1997.

Lanchester, B. S., Rees, M. H., Sedgemore, K. J. F., Palmer, J. R., Frey, H. U., and Kaila, K. U.: Ionospheric response to variable electric fields in small-scale auroral structures, Ann. Geophys., 16, 1343–1354, 1998, http://www.ann-geophys.net/16/1343/1998/.

Lanchester, B. S., Rees, M. H., Lummerzheim, D., Otto, A., Sedgemore-Schulthess, K. J. F., Zhu, H., and McCrea, I. W.: Ohmic heating as evidence for strong field-aligned currents in filamentary aurora, J. Geophys. Res., 106, 1785–1794, 2001.

Markkanen, J., Postila, M., and van Eyken, A.: Small-size debris data collection with EISCAT radar facilities, ESA Contract Report, June 2006.

McDade, I. C., Llewellyn, E. J., Murtagh, D. P., and Greer, R. G. H.: Eton 5: Simultaneous rocket measurements of the OH meinel $\Delta\upsilon$=2 sequence and (8,3) band emission profiles in the nightglow, Planet. Space Sci., 35, 1137–1147, doi:10.1016/0032-0633(87)90020-1, 1987.

McWhirter, I., Furniss, I., Lanchester, B. S., Robertson, S. C., Baumgardner, J., and Mendillo, M.: A new spectrograph platform for auroral studies on Svalbard, in: Proceedings of Atmospheric Studies by Optical Methods, pp. 1–4, 2001.

Pallamraju, D. and Chakrabarti, S.: First ground-based measurements of OI 6300 Å daytime aurora over Boston in response to the 30 October 2003 geomagnetic storm, Geophys. Res. Lett., 32, 3, doi:10.1029/2004GL021417, 2005.

Palmer, J. R.: Plasma density variations in aurora, PhD thesis, 1995.

Rees, M.: Physics and chemistry of the upper atmosphere, Cambridge University Press, 1989.

Rees, M. H., Abreu, V. J., and Hays, P. B.: The production efficiency of O+(2P) ions by auroral electron impact ionization, J. Geophys. Res., 87, 3612–3616, 1982.

Semeter, J.: Critical comparison of OII(732–733 nm), OI(630 nm), and N_2(1PG) emissions in auroral rays, Geophys. Res. Lett., 30, 1255, doi:10.1029/2002GL015828, 2003.

Semeter, J. and Blixt, E. M.: Evidence for Alfvén wave dispersion identified in high-resolution auroral imagery, Geophys. Res. Lett., 33, 13 106, doi:10.1029/2006GL026274, 2006.

Semeter, J., Lummerzheim, D., and Haerendel, G.: Simultaneous multispectral imaging of the discrete aurora, J. Atmos. Solar-Terr. Phys., 63, 1981–1992, 2001.

Sharpee, B. D., Slanger, T. G., Huestis, D. L., and Cosby, P. C.: Measurements of the Singly Ionized Oxygen Auroral Doublet Lines $\lambda\lambda$7320, 7330 Using High-Resolution Sky Spectra, Astrophys. J., 606, 605–610, doi:10.1086/382869, 2004.

Sivjee, G. G., Shen, D., Yee, J.-H., and Romick, G. J.: Variations, with peak emission altitude, in auroral O_2 atmospheric (1, 1)/(0, 1) ratio and its relation to other auroral emissions, J. Geophys. Res., 104, 28 003–28 018, 1999.

Sullivan, J. M., Lockwood, M., Lanchester, B. S., Kontar, E., Ivchenko, N., Dahlgren, H., and Whiter, D. K.: An optical study of multiple NEIAL events driven by low energy primary precipitation, Ann. Geophys., accepted, 2008.

Trondsen, T. S. and Cogger, L. L.: A survey of small-scale spatially periodic distortions of auroral forms, J. Geophys. Res., 103, 9405–9416, doi:10.1029/98JA00619, 1998.